physical sciences forum

MDPI

Proceeding Paper

Effect of Printing Direction on the Elastic Properties of 3D-Printed Nylon Materials †

Efstratios Polyzos [1,2,*] and Lincy Pyl [1]

[1] Department of Mechanics of Materials and Constructions, Vrije Universiteit Brussel (VUB), 1050 Brussels, Belgium
[2] Strategic Initiative Materials (SIM), Technologiepark 48, 9052 Zwijnaarde, Belgium
* Correspondence: efstratios.polyzos@vub.be
† Presented at the 19th International Conference on Experimental Mechanics, Kraków, Poland, 17–21 July 2022.

Abstract: Thermoplastic parts created using the Fused Filament Fabrication (FFF) technique exhibit transversely isotropic characteristics. The latter are associated with the development of bonds and voids between the printed filaments, both of which are an artifact of the FFF technique and can alter the elastic response of a part. In this study, 3D-printed nylon specimens are examined. The voids included in the specimens are visualized using micro-CT and the elastic properties are quantified by tensile tests. The micro-CT results illustrate that the voids are almost exclusively located between the printed filaments and obtain convex and concave shapes while presenting a limited volume fraction. Finally, the tensile tests indicate that the elastic properties are affected by the printing direction.

Keywords: 3D-printed thermoplastics; Fused Filament Fabrication; micro-CT; interbead voids

check for updates

Citation: Polyzos, E.; Pyl, L. Effect of Printing Direction on the Elastic Properties of 3D-Printed Nylon Materials. *Phys. Sci. Forum* **2022**, *4*, 21. https://doi.org/10.3390/psf2022004021

Academic Editors: Zbigniew L. Kowalewski and Elżbieta Pieczyskaz

Published: 11 August 2022

1. Introduction

Additive manufacturing (or 3D printing) is a relatively new manufacturing technology that offers significant advantages owing to design flexibility and the ability to produce lightweight parts [1].

The Fused Filament Fabrication (FFF) technique is among the most upcoming 3D-printing techniques used for the production of thermoplastic parts. The FFF thermoplastic parts are comprised of successively printed thermoplastic filaments, otherwise known as beads, which are extruded through a heated nozzle in a malleable condition according to a computer design and deposited layer-by-layer on a printbed. Acrylonitrile butadiene styrene (ABS), polylactic acid (PLA), polyamide (PA), and nylon are some of the commonly used materials [2].

The simplicity with which these materials may be printed comes at the expense of performance as the 3D-printed thermoplastics exhibit lower mechanical properties compared to metals or composite materials. A key method of improving their performance is the addition of continuous fibers in the thermoplastic matrix. In particular, the addition of continuous Kevlar, glass, and carbon fibers has shown a significant improvement in mechanical properties. Currently, high-end 3D printers able to print with reinforced thermoplastics, such as the Markforged Mark Two, are commercially available [3].

High-end printers typically add by default a protective layer around each part, aiming to ameliorate its external surface. Eiger software, as used by Markforged [4] for the geometry slicing process, clearly specifies that items with an insufficient external cover layer size have a lower surface quality. Lower surface quality increases stress concentrations in certain areas, thus decreasing the overall performance of the produced parts. The protective cover is printed around the reinforced infill and consists of the floor and roof layers, both printed using a 45° printing pattern, and the wall layers, printed using a 0° pattern. As a result, the finished 3D-printed parts are a mix of unreinforced matrix cover layers and reinforced infill material. An illustration of the FFF structure is depicted in Figure 1.

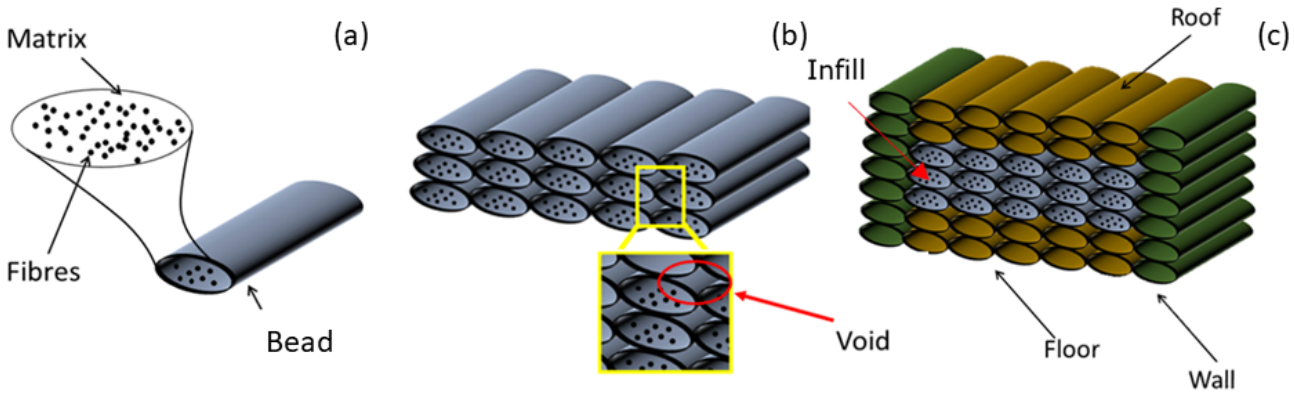

Figure 1. Example of the printing process of an FFF reinforced thermoplastic part. (**a**) Single reinforced bead; (**b**) ensemble of reinforced beads (infill); (**c**) infill enclosed in protective cover constituted by the roof, floor, and wall layers [2].

In numerical schemes, the mechanical properties, and in particular, the elastic properties, of the unreinforced layers are mostly assumed to be isotropic. Researchers used either the elastic properties of printed specimens [5] or of unprinted nylon [2] to simulate the elastic response of the unreinforced layers. However, both of the preceding assumptions can lead to major modeling errors since the elastic properties of the final printed part are heavily influenced by the manufacturing process.

Even though the properties of the initial unprinted nylon are indeed isotropic, the 3D-printed parts manufactured by the FFF technique have been observed to express transversely isotropic characteristics. The deviation in the properties from the isotropic case is primarily attributed to the non-uniform bonding patterns that are formed along the path of the bead [6,7].

The transverse isotropy can be additionally affected by the geometry and the fraction of the existent voids. The primary cause of porosity in 3D-printed FFF parts is the presence of the interbead voids generated due to the ellipsoidal cross-sectional shape of the beads. Those voids run parallel to the beads and are highly affected by the material properties and the printing path [6,8]. The interbead voids are illustrated in Figure 1b. Voids of structures consisting of materials such as ABS have been extensively studied [6,9,10], whereas structures of nylon have not been similarly investigated.

Both the void geometry and shape and the elastic properties of the 3D-printed materials are components critical for the modeling of reinforced and unreinforced structures and require further exploration.

This research is focused on achieving two specific goals. Firstly, to visualize the voids in 3D-printed nylon structures to aid the understanding of the void formation. Secondly, to examine the elastic properties of 3D-printed nylon structures that correspond to the orientations used for the roof and floor ($\pm 45^\circ$) as well as walls (0° and 90°) of the external cover, and to investigate the cause of transverse isotropy in 3D-printed nylon.

2. Materials

All samples were created by the Mark Two 3D printer (Markforged: Watertown, MA, USA) using a nylon filament (or "Nylon End-of-Life") and the default setting for nozzle temperature (275°) and speed (9.2 mm/s), with the specifications of a solid fill and isotropic pattern. The filaments were obtained from AMR Europe, a feedstock provider for Markforged. Following the standard printing process, a stereolithography (STL) 3D geometry was prepared in ABAQUS [11] and later imported into the Markforged Eiger software (Markforged: Watertown, MA, USA) for slicing.

The manufacturing of parts with orientations, such as the roof, floor, and wall, requires the printing of two structures. Structure 45, illustrated in Figure 2a, was directly printed in a ready-to-test form, as described in the ASTM [12], using the default $\pm 45^\circ$ printing

orientation of Markforged's Eiger software. These specimens were designed to identify the properties of the roof and floor, which are printed by default using this orientation.

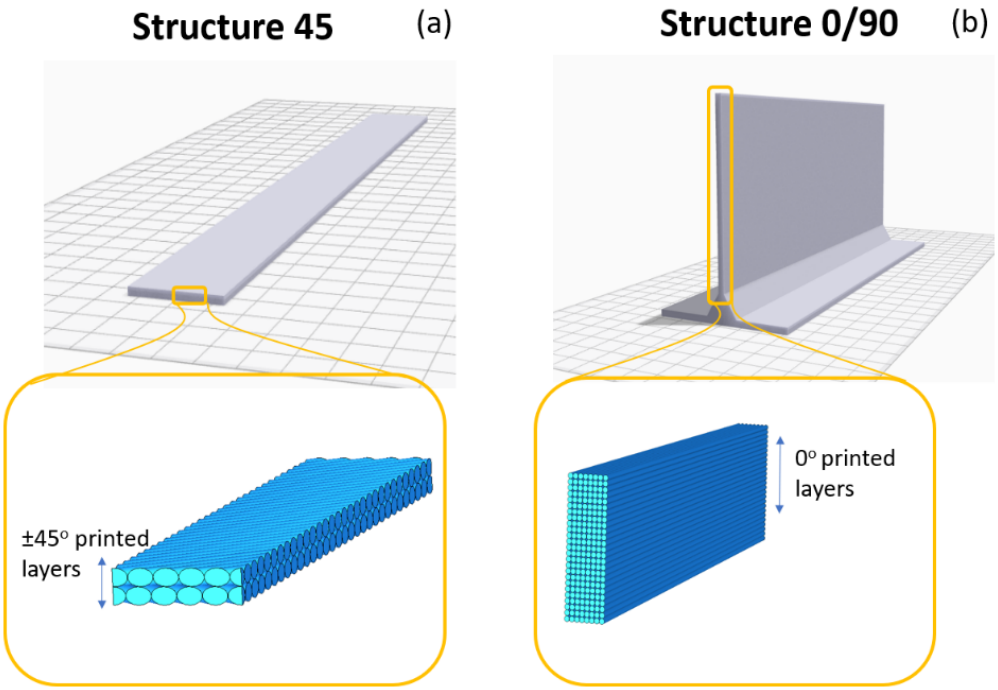

Figure 2. The geometry of the different printed structures. (**a**) Structure 45 containing the ±45° printed layers; (**b**) Structure 0/90 containing the 0° printed layers.

Unfortunately, the limitations of the printing pattern obstruct the simple manufacturing of similar 0° and 90° specimens since the user is unable to print rectangular nylon specimens using 0° and 90° printing patterns in Markforged's Eiger software. To address this issue, Structure 0/90 was printed vertically using a contour pattern that was likewise employed in the creation of the walls during the printing of the reinforced parts (Figure 2b). A triangular base support structure was additionally added to minimize severe warping—a common problem of slender 3D-printed thermoplastics. The base structure was removed after printing using a diamond saw and five additional specimens were shaped out of the rectangular plate for each of the 0° and the 90° orientations (Figure 3). The 0° specimens were cut following a direction parallel to the printing pattern, whereas a direction normal to the printing pattern was used for the 90° specimens. The width, length, and thickness of all specimens (illustrated in Figure 3 (c_1) and (c_2)) were 25, 250, and 2 mm, respectively.

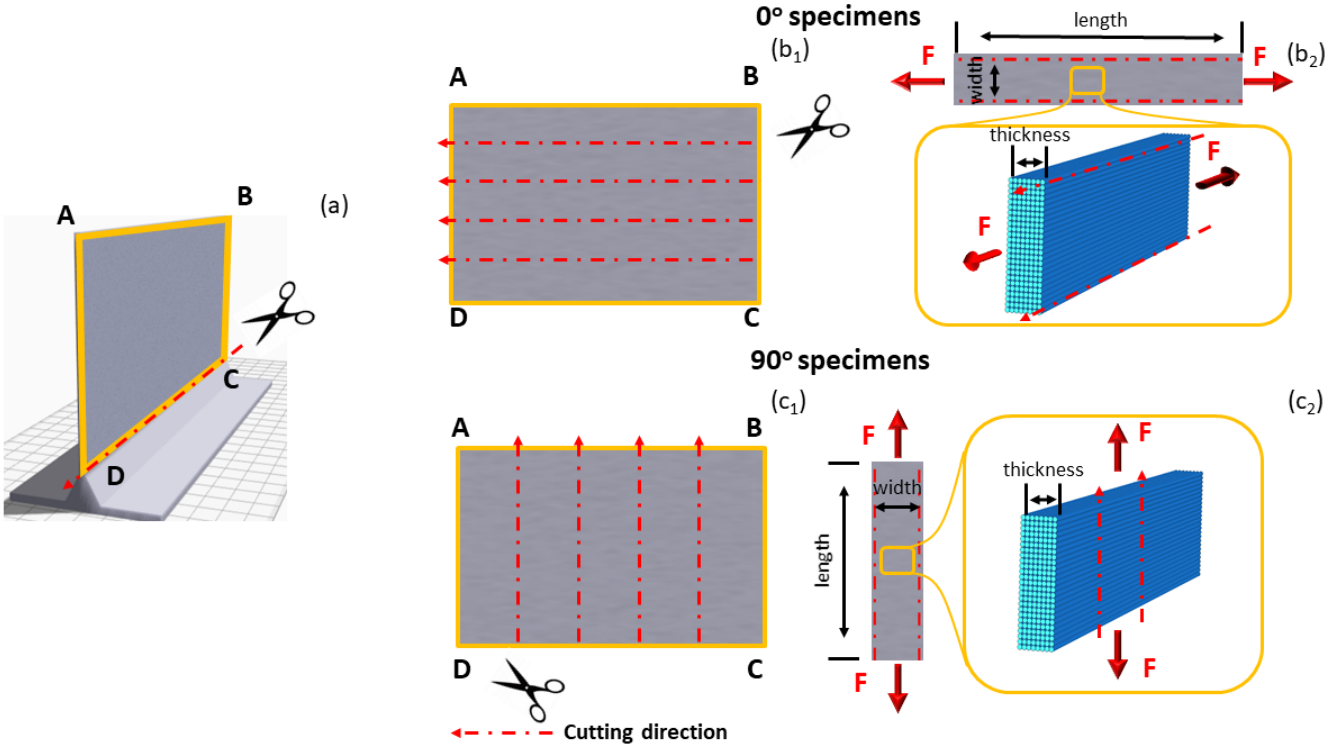

Figure 3. Preparation of the 0° and 90° specimens: (**a**) removal of the base; (**b1**,**c1**) the cutting direction of the 0° and 90° specimens, respectively; (**b2**,**c2**) the loading direction and internal printing pattern of the 0° and 90° specimens, respectively.

3. Testing Equipment and Process

An Instron 5885 H (Instron, Norwood, MA, USA) tensile testing machine was employed for testing the specimens in tension. All specimens were tightly attached using pneumatic clamps to eliminate artificial torsion effects and tested using a 10-kN loadcell. The rectangular specimens were loaded along the long side, as illustrated in Figure 3, panels (b_2) and (c_2). A DIC (Digital Image Correlation) system with two Stingray Cameras of 5 MP and 23 mm lenses were used to obtain the surface strains, and VIC-3D, by Correlated Solutions, was used to process the DIC data. Note that an appropriate speckle pattern was applied to every specimen prior to its testing.

The void fraction and shape were investigated using a Bruker Skyscan micro-CT scanner (Billerica, MA, USA). Bruker's CTAn (CT-Analyzer) 1.14 software was utilized for processing and displayed the resulting 4K images through surface rendering. The void fraction was calculated using CTAn's built-in technique, which extracts data from binarized files of specified volume sections of the structure. The measurements of the porosity are sensitive to edge roughness potentially caused by the specimens' post-processing. Therefore, the roughened portions adjacent to the edges were not considered for void fraction measurement. Bruker's CTVox (CT-Voxel) 3.0 software was utilized for volume rendering and void geometry visualization.

4. Results and Discussion

The findings considering the stress–strain curves of the three groups of specimens of 0°, ±45°, and 90° are summarized in Figure 4. A magnification is offered for the elastic region below 1% strain to aid the visualization of the results. Young's modulus and Poisson's ratio for each group were evaluated using the standardized process [12]. The results considering the mean and the standard deviation of Young's modulus and Poisson's ratio for the five specimens of each group are summarized in Table 1.

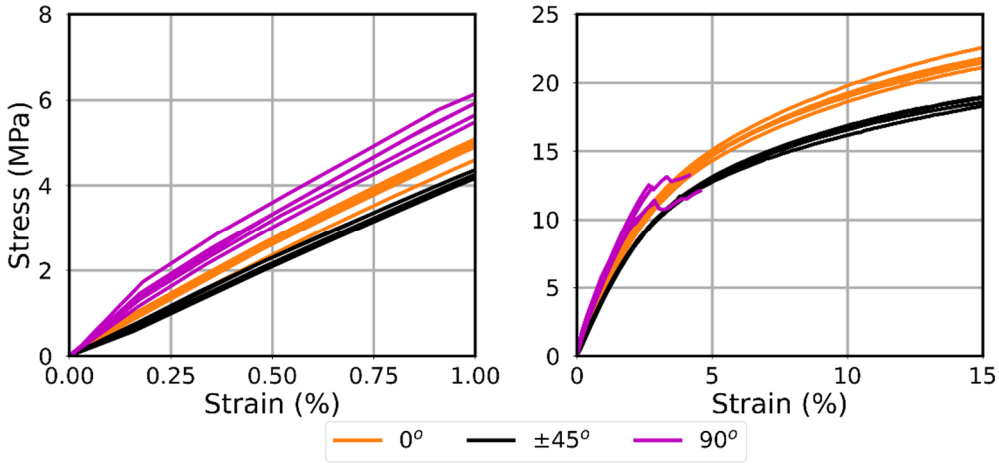

Figure 4. Stress–strain curves of the 0°, ±45°, and 90° specimens up to 1% and 15% strain.

Table 1. Young's modulus (GPa) and Poisson's ratio (−) for the 0°, ±45°, and 90° specimens.

	0° Specimen	**±45° Specimen**	**90° Specimen**
Young's modulus (GPa)	0.48 ± 0.02	0.42 ± 0.02	0.53 ± 0.02
Poisson's ratio (−)	0.42 ± 0.02	0.40 ± 0.05	0.45 ± 0.03

One-way ANOVA (analysis of variance) was used to compare the Young's moduli of the three groups of specimens. The results depict a statistically significant difference in the means at a 95% significance level (p-value $< 1 \times 10^{-7}$). Since the one-way ANOVA is an omnibus test statistic, the post-hoc single-step multi-comparison Tukey's HSD (honestly significant difference) test was conducted to determine the group pairs that differ significantly, by comparison of all pairs of means. The results depict that there is a statistically significant difference between all pairs of groups (p-value $< 1 \times 10^{-3}$), therefore confirming that the elastic behavior of the material depends on the printing orientation and thus the modeling schemes should use the appropriate properties. In particular, the longitudinal elastic modulus of the roof and floor layers (±45° specimens) should not be used for the walls (0° specimens) since they differ by 16.3%. The difference is further amplified when comparing the Young's modulus of the roof and floor layers to the transverse elastic modulus of the walls (90° specimens), which differ by 31.8%.

On the other hand, implementing the ANOVA test for the findings of Poisson's ratio demonstrates that there is no statistically significant difference between the mean values of the three groups at a 95% confidence level.

In the literature, the Young's modulus of the 3D-printed nylon specimens fabricated by Markforged printers has been reported in the range 0.29–0.9 GPa [13–16], with the majority of the studies reporting results near the lower end of the range [14–16]. In this regard, the measurements of this study are well in agreement with those presented in the literature. Finally, it is important to underline that the 3D-printed specimens exhibit a different performance in comparison to the extruded nylon (Young's modulus 0.35–3.5 GPa) [17,18]. This result has been previously linked to the bonding between the beads and the calorimetric behavior of the printable materials [19]. For the present case, an indication of the bonding capacity is the exhibition of a brittle fracture by the 90° specimens, which are loaded normally in the printing direction.

The reconstructed view of the 3D geometry using CTVox for Structure 45 and Structure 0/90 is shown in Figure 5. The micro-CT scan displays a void architecture that mimics long cylinders stretching parallel to the beads and positioned at regular intervals. In Structure 0/90, the distance between layers of the voids is roughly proportional to the height of each bead, whilst in Structure 45 to the thickness of the bead. For Structure 45, the alternate ±45° layers are evident. The shape of the voids is both concave and convex in Structure

0/90, while in Structure 45 a convex shape is more prominent. Magnification images of the voids were added in Figure 5 to aid the visualization of the voids' shape.

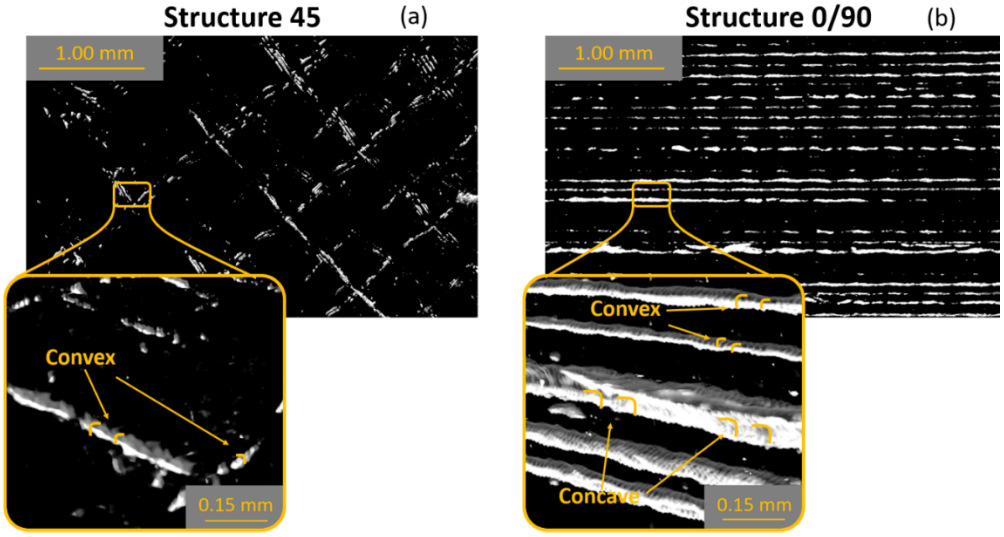

Figure 5. Micro-CT images of the voids (depicted in white) within the nylon matrix (depicted in black) for (**a**) Structure 45 and (**b**) Structure 0/90.

The void fraction of Structure 45 is approximately 0.07% and 0.10% for Structure 0/90, which is low compared to other printed materials. For example, printed ABS 0° specimens have a void fraction of 6.9% when printed using the same printing pattern and similar printing parameters (270° printing temperature and 12.7 mm/s printing speed).

The differences in elastic properties have previously been attributed to voids generated during the specimen production process [2]. However, given the low overall porosity in the nylon specimens, the existence of voids is unlikely to be the source of the transverse isotropy. As a result, the bond established between neighboring beads is most likely the reason for the final part's transversely isotropic character. This statement is further supported by analytical and numerical models for structures containing such voids [7]. Furthermore, this bond is likely the cause of the deviation noted between the tensile and flexural behavior of the printed parts [20]. Even in reinforced specimens tested in delamination, where the specimens are primarily under flexion [21], the drop in Young's modulus is approximately 35% [22]. The above require further study on the influence of the bond on the mechanical properties of 3D-printed parts to quantify its effects.

5. Conclusions

The current article investigates the elastic properties of 3D-printed materials. The elastic properties of the nylon specimens were printed in the 0°, ±45°, and 90° orientation patterns and tested in tension, demonstrating an orientational dependency. Micro-CT scanning was used to evaluate the void shape and void fraction. Convex and concave voids were visualized to run parallel to the printing direction. The porosity of all the observed structures was less than 1%, and the tensile specimens' transverse isotropy was attributed to bond formation between the neighboring beads.

Considering the above, two important conclusions can be extracted from the present work. Firstly, the bond between the adjacent beads will lead to final parts with transversely isotropic properties. Secondly, even with very low void concentrations, the final printed part must be regarded as transversely isotropic.

Author Contributions: Conceptualization, E.P. and L.P.; methodology, E.P.; software, E.P.; validation, E.P.; formal analysis, E.P.; investigation E.P.; resources, L.P.; data curation, E.P.; writing—original draft preparation, E.P.; writing—review and editing, E.P. and L.P.; visualization, E.P.; supervision, L.P.; project administration, L.P.; funding acquisition, L.P. All authors have read and agreed to the published version of the manuscript.

Funding: This research was funded by SIM (Strategic Initiative Materials) in Flanders (award number HBC.2017.0321), VLAIO (Flanders Agency for Innovation and Entrepreneurship), and Fonds voor Wetenschappelijk Onderzoek—Vlaanderen (FWO) (award number 1102822N).

Institutional Review Board Statement: Not applicable.

Informed Consent Statement: Not applicable.

Acknowledgments: The authors gratefully acknowledge SIM (Strategic Initiative Materials) in Flanders and VLAIO (Flanders Agency for Innovation & Entrepreneurship) for their support of the SBO project RELFICOM, part of the Nanoforce Program. Additionally, the financial contribution of the FWO Research Foundation–Flanders (file number 1102822N) is gratefully acknowledged.

Conflicts of Interest: The authors declare no conflict of interest.

References

1. Brenken, B.; Barocio, E.; Favaloro, A.; Kunc, V.; Pipes, R.B. Fused filament fabrication of fiber-reinforced polymers: A review. *Addit. Manuf.* **2018**, *21*, 1–16. [CrossRef]
2. Polyzos, E.; Katalagarianakis, A.; Polyzos, D.; Van Hemelrijck, D.; Pyl, L. A multi-scale analytical methodology for the prediction of mechanical properties of 3D-printed materials with continuous fibres. *Addit. Manuf.* **2020**, *36*, 101394. [CrossRef]
3. van de Werken, N.; Tekinalp, H.; Khanbolouki, P.; Ozcan, S. Additively manufactured carbon fiber-reinforced composites: State of the art and perspective. *Addit. Manuf.* **2020**, *31*, 100962. [CrossRef]
4. Markforged, Nylon Material Datasheet. 2022. Available online: https://www-objects.markforged.com/craft/materials/CompositesV5.2.pdf (accessed on 3 August 2022).
5. Dutra, T.A.; Ferreira, R.T.L.; Resende, H.B.; Guimaraes, A. Mechanical characterization and asymptotic homogenization of 3D-printed continuous carbon fiber-reinforced thermoplastic. *J. Braz. Soc. Mech. Sci. Eng.* **2019**, *41*, 1–15. [CrossRef]
6. Rodríguez, J.F.; Thomas, J.P.; Renaud, J.E. Mechanical behavior of acrylonitrile butadiene styrene fused deposition materials modeling. *Rapid Prototyp. J.* **2003**, *9*, 219–230. [CrossRef]
7. Polyzos, E.; Ravidranath, S.B.; Van Hemelrijck, D.; Pyl, L. Analytical and numerical modelling of voids in additively manufactured thermoplastic parts. *Addit. Manuf.* **2021**, *48*, 102356. [CrossRef]
8. Polyzos, E.; Van Hemelrijck, D.; Pyl, L. Numerical modelling of the elastic properties of 3D-printed specimens of thermoplastic matrix reinforced with continuous fibres. *Compos. Part B Eng.* **2021**, *211*, 108671. [CrossRef]
9. Rodríguez, J.F.; Thomas, J.P.; Renaud, J.E. Mechanical behavior of acrylonitrile butadiene styrene (ABS) fused deposition materials. Experimental investigation. *Rapid Prototyp. J.* **2001**, *7*, 148–158. [CrossRef]
10. Rodríguez, J.F.; Thomas, J.P.; Renaud, J.E. Design of fused-deposition ABS components for stiffness and strength. *J. Mech. Des.* **2003**, *125*, 545–551. [CrossRef]
11. *ABAQUS/Standard User's Manual*; Version 6.9; Dassault Systèmes Simulia Corp: Providence, RI, USA, 2009.
12. *ASTM D3039*; Standard Test Method for Tensile Properties of Polymer Matrix Composite Materials. ASTM International: West Conshohocken, PA, USA, 2000.
13. Van Der Klift, F.; Koga, Y.; Todoroki, A.; Ueda, M.; Hirano, Y.; Matsuzaki, R. 3D printing of continuous carbon fibre reinforced thermo-plastic (CFRTP) tensile test specimens. *Open J. Compos. Mater.* **2016**, *6*, 18–27. [CrossRef]
14. Dickson, A.N.; Barry, J.N.; McDonnell, K.A.; Dowling, D.P. Fabrication of continuous carbon, glass and Kevlar fibre reinforced polymer composites using additive manufacturing. *Addit. Manuf.* **2015**, *16*, 146–152. [CrossRef]
15. Naranjo-Lozada, J.; Ahuett-Garza, H.; Orta-Castañón, P.; Verbeeten, W.M.; Sáiz-González, D. Tensile properties and failure behavior of chopped and continuous carbon fiber composites produced by additive manufacturing. *Addit. Manuf.* **2019**, *26*, 227–241. [CrossRef]
16. Chabaud, G.; Castro, M.; Denoual, C.; Le Duigou, A. Hygromechanical properties of 3D printed continuous carbon and glass fibre reinforced polyamide composite for outdoor structural applications. *Addit. Manuf.* **2019**, *26*, 94–105. [CrossRef]
17. Melenka, G.W.; Cheung, B.K.; Schofield, J.S.; Dawson, M.R.; Carey, J.P. Evaluation and prediction of the tensile properties of continuous fiber-reinforced 3D printed structures. *Compos. Struct.* **2016**, *153*, 866–875. [CrossRef]
18. Matweb. 2020. Available online: http://www.matweb.com/ (accessed on 3 August 2022).
19. Pascual-González, C.; Iragi, M.; Fernández, A.; Fernández-Blázquez, J.P.; Aretxabaleta, L.; Lopes, C.S. An approach to analyse the factors behind the micromechanical response of 3D-printed composites. *Compos. Part B Eng.* **2020**, *186*, 107820. [CrossRef]
20. Yu, T.; Zhang, Z.; Song, S.; Bai, Y.; Wu, D. Tensile and flexural behaviors of additively manufactured continuous carbon fiber-reinforced polymer composites. *Compos. Struct.* **2019**, *225*, 111147. [CrossRef]

21. Polyzos, E.; Van Hemelrijck, D.; Pyl, L. Analytical model for the estimation of the hygrothermal residual stresses in generally layered laminates. *Eng. Fract. Mech.* **2021**, *247*, 107667. [CrossRef]
22. Polyzos, E.; Katalagarianakis, A.; Van Hemelrijck, D.; Pyl, L. Delamination analysis of 3D-printed nylon reinforced with continuous carbon fibres. *Addit. Manuf.* **2021**, *46*, 102144. [CrossRef]